RESEARCH ARTICLE

3D ultrastructural organisation of calcium release units in the avian sarcoplasmic reticulum

Thomas M. D. Sheard[1],*, Sanjay R. Kharche[1,2,3], Christian Pinali[1] and Holly A. Shiels[1],‡

ABSTRACT

Excitation–contraction coupling in vertebrate hearts is underpinned by calcium (Ca^{2+}) release from Ca^{2+} release units (CRUs). CRUs are formed by clusters of channels called ryanodine receptors on the sarcoplasmic reticulum (SR) within the cardiomyocyte. Distances between CRUs influence the diffusion of Ca^{2+}, thus influencing the rate and strength of excitation–contraction coupling. Avian myocytes lack T-tubules, so Ca^{2+} from surface CRUs (peripheral couplings, PCs) must diffuse to internal CRU sites of the corbular SR (cSR) during centripetal propagation. Despite this, avian hearts achieve higher contractile rates and develop greater contractile strength than many mammalian hearts, which have T-tubules to provide simultaneous activation of the Ca^{2+} signal through the myocyte. We used 3D electron tomography to test the hypothesis that the intracellular distribution of CRUs in the avian heart permits faster and stronger contractions despite the absence of T-tubules. Nearest edge–edge distances between PCs and cSR, and geometric information including surface area and volume of individual cSR, were obtained for each cardiac chamber of the white leghorn chicken. Computational modelling was then used to establish a relationship between CRU distance and cell activation time in the avian heart. Our data suggest that cSR clustered close together along the Z-line is vital for rapid propagation of the Ca^{2+} signal from the cell periphery to the cell centre, which would aid in the strong and fast contractions of the avian heart.

KEY WORDS: Bird, Chicken, Computational model, Calcium diffusion, Electron tomography, Peripheral coupling

INTRODUCTION

The four-chambered avian heart possesses many similarities to its mammalian counterpart. Both groups independently evolved a fully divided ventricle, capable of producing fast contractile rates with robust pressure development. However, despite similarities in cardiac performance and gross organ morphology, there are substantial differences on a cellular and subcellular level within the cardiomyocytes. Avian atrial and ventricular myocytes are long (>100 μm) and thin (3–9 μm), with a small cross-sectional area (~56 μm²) and cell volume (~10 pl); these features provide a large surface area to volume ratio (Akester, 1981; Bogdanov et al., 1995;

[1]University of Manchester, Faculty of Biology, Medicine and Health, Core Technology Facility, 46 Grafton Street, Manchester M13 9NT, UK. [2]Department of Medical Biophysics, University of Western Ontario, London, ON, N6A 3K7, Canada. [3]Lawson Health Research Institute, 800 Commissioners Road East, London, ON, N6C 2R5, Canada.
*Present address: University of Leeds, Garstang Building, Woodhouse Lane, Leeds LS2 9JT, UK.

‡Author for correspondence (holly.shiels@manchester.ac.uk)

T.M.D.S., 0000-0003-4940-3188; S.R.K., 0000-0002-2634-4894; C.P., 0000-0001-9815-6940; H.A.S., 0000-0001-5223-5205

Dzialowski and Crossley, 2015). It is likely that these morphological features allow excitation–contraction coupling to work within the necessary timescale without sarcolemmal invaginations, known as T-tubules (Sommer and Johnson, 1969). T-tubules are found in all mammalian ventricular myocytes and in atrial myocytes of large mammals, and are important for synchronised depolarisation in these larger cells (Dibb et al., 2009). The lack of T-tubules, characteristic of ectothermic vertebrates (fish, amphibians and non-avian reptiles), has been associated with slower heart rates and less robust contractile function (Shiels and Galli, 2014). We hypothesise that the subcellular organisation of calcium (Ca^{2+}) release units (CRUs) within the avian myocyte may reconcile this apparent enigma.

Contraction and relaxation of the heart is underpinned by Ca^{2+} cycling in the cardiomyocytes. Following membrane depolarisation, Ca^{2+} enters the cell via voltage-gated L-type Ca^{2+} channels (LTCC). The initial Ca^{2+} that enters via LTCCs induces further Ca^{2+} release from the intracellular stores of the sarcoplasmic reticulum (SR), in a process called Ca^{2+}-induced Ca^{2+} release (CICR). SR Ca^{2+} is released by the ryanodine receptor (RyR) channels, which cluster in structures defined as CRUs. In birds, there are two types of CRU. The first are peripheral couplings (PCs), which are clusters of RyRs on the surface of junctional SR (jSR), directly adjacent to sarcolemmal LTCCs. The second type of CRU is formed by RyR clusters which are not associated with the surface sarcolemma, known as corbular SR (cSR). cSR are shorter, rounder segments of SR than those found at the PCs. Despite being positioned micrometres from the sarcolemma (Sommer, 1995), these internal CRUs contribute to global Ca^{2+} release and are necessary for robust excitation–contraction coupling (Franzini-Armstrong et al., 2005). Ca^{2+} released at PCs must diffuse centripetally to the cSR/EjSR. Ca^{2+} is taken up by contracting myofilaments and adjacent mitochondria, or can be buffered in the cytosol, and thus [Ca^{2+}] falls rapidly the further it travels from a CRU (Sobie et al., 2006). The distribution of CRUs, as well as the depletion of SR Ca^{2+} stores, ensures that excitation–contraction coupling is not endlessly regenerative and unstable, a situation that would be pro-arrhythmic and deleterious to the myocyte (Cannell et al., 1995).

There is a limited amount of functional data on Ca^{2+} flux pathways in avian cardiomyocytes. [³H]ryanodine binding studies in pigeon and finch left ventricle (LV) indicate that the density and Ca^{2+} sensitivity of RyRs are similar to those of mammalian RyRs (Junker et al., 1994). An early study showed a high density of LTCC current and a prominent T-type Ca^{2+} channel current in whole-cell voltage-clamped finch ventricular myocytes (Bogdanov et al., 1995), which the authors suggested could aid in CICR in the absence of T-tubules. This same study reported faster inactivation kinetics of I_{Ca} in finch compared with rat myocytes and suggested that this may facilitate fast heart rates.

We are unaware of studies that quantify the dynamics of avian intracellular Ca^{2+} movement directly (Kim et al., 2000), but it is

List of abbreviations

CICR	calcium-induced calcium release
CRU	calcium release unit
cSR	corbular SR
d_1	distance between PCs
d_2	distance between Z-lines
d_3	distance between cSR along a Z-line
EjSR	extended junctional SR
ET	electron tomography
fSR	free SR
jSR	junctional SR
LA	left atrium
LTCC	L-type calcium channel
LV	left ventricle
PC	peripheral coupling
RA	right atrium
RV	right ventricle
RyR	ryanodine receptor
SR	sarcoplasmic reticulum
TEM	transmission electron microscopy

possible to speculate on this by examining Ca^{2+} cycling in other cells that are similar in structure. Ectotherm cardiomyocytes, mammalian neonatal cardiomyocytes and mammalian nodal and Purkinje cells also lack T-tubules and tend to be thinner in diameter than mammalian ventricular cardiomyocytes. Studies from these cell types show that Ca^{2+} levels rise rapidly at the periphery, followed by a time-dependent rise in the cell centre (Boyden et al., 2000; Woo et al., 2003; Shiels and White, 2005; Stuyvers et al., 2005; Louch et al., 2015).

Our current understanding of the structural organisation of the Ca^{2+} release system in birds discussed above has been characterised using 2D transmission electron microscopy (TEM) (Franzini-Armstrong et al., 1999; Perni et al., 2012). However, a more realistic representation of the CRU distribution in space can be achieved with 3D electron microscopy. In this study, we characterised the distribution of CRUs in myocytes from each of the four chambers of the heart of the white leghorn chicken (*Gallus gallus domesticus*) using electron tomography (ET). This technique enables the reconstruction and visualisation of subcellular organisation of the SR network in a detailed 3D structure. Tomograms from both atria and both ventricles were reconstructed, and the structures of interest were segmented to (1) study the nearest edge–edge distances between PCs and between the cSR; and (2) obtain cSR volume and surface area to determine Ca^{2+} capacity and RyR cluster size. These inter-CRU distances were used to inform a computer model of Ca^{2+} wave dynamics which tested the effect of inter-CRU distance on whole-cell Ca^{2+} activation.

MATERIALS AND METHODS
Tissue samples and specimen preparation
Three adult chickens [white leghorn variety, *Gallus gallus domesticus* (Linnaeus 1758); 1.5–2 kg in body mass] were acquired from Hinchliffe's Farm, Huddersfield, UK. White leghorns are a slow-growing bird, bred for egg production with no pre-disposition to cardiac dysfunction (Mirsalimi et al., 1993). Chickens were transported to the University of Manchester Biological Services Facility, where they were humanely killed with pentobarbital, followed by dislocation of the neck in accordance with the Animals (Scientific Procedures) Act 1986. Hearts were excised, and tissue from each of the four chambers (left atrium, LA; right atrium, RA; left ventricle, LV; right ventricle, RV) was cut into 1 mm³ samples and

placed into Karnovsky fixative with $CaCl_2$ (2% formaldehyde, 2.5% glutaraldehyde, 50 mmol l⁻¹ $CaCl_2$, 0.1 mol l⁻¹ Hepes). Tissue preparation was according to the Ellisman protocol (Deerinck et al., 2010). All reagents were obtained from Sigma.

Sectioning was carried out on a Reichert-Jung UltraCut E ultramicrotome using a glass knife. Sections of ~100 nm thickness (gold coloured ribbons) were produced for observation using a FEI Tecnai 12 Bio Twin transmission electron microscope operated at 100 kV to assess tissue preparation prior to ET.

Electron tomography
ET was performed using an FEI Tecnai G2 Polara transmission electron microscope at the University of Manchester Electron Microscopy Facility, operated at 300 kV using magnifications of approximately ×10,000, ×12,000 and ×15,500. For ET, sections of ~400 nm thickness (green/purple coloured ribbons) were collected on 200 mesh grids; 10 nm gold fiducial markers were added to the sections to aid tilt series collection, alignment and dataset reconstruction. Tilt series were taken at areas where the myofibrils were longitudinal, as this aids the identification of the cSR. Single-axis tilt series were acquired at 1 deg intervals from −60 to +60 deg, or as close to this maximal angle range as possible. Tilt series were obtained from multiple cells within each of the atria and ventricles for all individuals. Alignment, reconstruction and segmentation were performed in the open-source software package *IMOD* (Kremer et al., 1996). *eTomo* was used for alignment and reconstruction, and *3dmod* was used to view the tomograms, segment the structures of interest and obtain the distance, volume and surface area measurements from the 3D reconstructions.

Following manual segmentation, the edge–edge distances between the CRUs were measured. PCs were identified as specialised regions of SR in close apposition (10–15 nm) to the sarcolemma (Junker et al., 1994), while cSR were identified as spherical structures (~100 nm in diameter) attached to the SR network, predominantly found along Z-lines (Asghari et al., 2009). Nearest edge–edge distances between PCs and between cSR were obtained from *IMOD* by drawing a line in the tomogram volume between the segmented CRUs. Nearest edge–edge distances are important for understanding cellular Ca^{2+} dynamics as they indicate the minimum distance that must be crossed by Ca^{2+} released at one site in order to act on an adjacent site (Perni et al., 2012). As cSR are distributed around the Z-lines, we measured distances between cSR distributed around the same Z-line. Geometric data regarding individual cSR were obtained by fully segmenting each cSR in every slice of each tomogram.

Computational methods
Model geometry
A 2D Ca^{2+} wave model representing an avian cardiomyocyte was constructed to assess the relationship between inter-CRU distance and whole-cell Ca^{2+} activation time. The myocyte was constructed as 8 µm wide (y-axis) and 136 µm long (x-axis) (Kim et al., 2000). PCs were placed at regular intervals along the cell membrane in the x-direction; Z-lines were placed at regular intervals along the x-axis and extended across the y-axis; and cSR were placed at regular intervals on the Z-lines (see Fig. 5A). The model geometry was discretised at a space step of 0.05 µm and thus PCs were placed at a depth from the cell membrane of 50 nm. This is greater than the biological distance (~10–15 nm) but we were required to accept this limitation because of the computational power required to provide finer discretisation. CRUs were separated by distances d_1 (distance between PCs), d_2 (distance between Z-lines) and d_3 (distance

between cSR along a Z-line). These distances were varied in a systematic way to encompass the range of values measured in the tomogram datasets. Distance d_1 was tested at 0.25, 0.5 and 0.75 µm, d_3 at 0.1, 0.2, 0.4 and 0.6 µm, and d_2 was varied to represent Z-line spacing indicative of a myocyte at rest (1.7–1.9 µm), as well as encompassing values that could be achieved during myocardial stretch (2.1 µm) and myocardial contraction (1.5 µm). The distance ranges are tabulated in Table S1.

Ca²⁺ dynamics model

The Ca²⁺ dynamics model was adapted from previous models (Cheng et al., 1993; Smith et al., 1998; Izu et al., 2001). CRU activation began at the surface sarcolemma and moved towards the centre of the cell. Cell membrane activation initiated propagation of the Ca²⁺ wave in the y-direction. At t=0, [Ca²⁺] was raised to 100 µmol l⁻¹ at y=0 µm and y=8 µm for 1 ms. Ca²⁺ dynamics were then permitted to evolve for the duration of one heartbeat (225 ms), according to the equations given below (see 'Model equations for Ca²⁺ wave propagation simulations'). Whole-cell activation was achieved when all grid locations reached a [Ca²⁺] value of 100 µmol l⁻¹ or more at least once (as per Smith et al., 1998; Izu et al., 2001). Ca²⁺ release was simulated as a stochastic process; release at a CRU occurred when local [Ca²⁺] exceeded 0.1 µmol l⁻¹ as described previously (Smith et al., 1998). The probability of a given CRU being open was assumed to be proportional to J_{pump}, the Ca²⁺ resequestration flux by Ca²⁺ ATPases located on the CRUs (Smith et al., 1998) (see below). Once a CRU was open, it was permitted to release Ca²⁺ for 10 ms (Smith et al., 1998). The spatial network of CRUs were diffusively coupled to permit simulation of Ca²⁺ waves (Izu et al., 2001).

The effect of mobile buffers was omitted. This may affect the absolute slope of the relationship between Ca²⁺ activation time and the distance between CRUs, but is not expected to impact the relative effect of changing distance (d_1, d_2 and d_3) on activation time.

Robust implicit finite difference solvers developed previously (Kharche et al., 2017) were used to solve the reaction–diffusion equations using a maximum temporal step of 0.02 ms (Table S1). Ten simulations were performed for each combination of distances (d_1, d_2, d_3), and an average activation time from the 10 simulations was taken to form each data point. Parallelisation was implemented using message passing interface (MPI). Each simulation required 24 processors 4 h to complete.

Model equations for Ca²⁺ wave propagation simulations

Model equations were derived from those found in Smith et al. (1998):

$$\frac{\partial[Ca^{2+}]_i}{\partial t} = D_c \nabla^2[Ca^{2+}]_i + J_n + J_{pump} + J_{leak} + J_{ryr}, \quad (1)$$

where D_c is the diffusion coefficient of free Ca²⁺, J_n is the flux due to immobile buffers, J_{pump} is the Ca²⁺ resequestration flux by Ca²⁺ ATPases located on the CRUs, J_{leak} is the magnitude of the SR leak and J_{ryr} is the Ca²⁺ released via the CRU;

$$\frac{\partial[CaB_n]}{\partial t} = -J_n (\text{immobile buffers}), \quad (2)$$

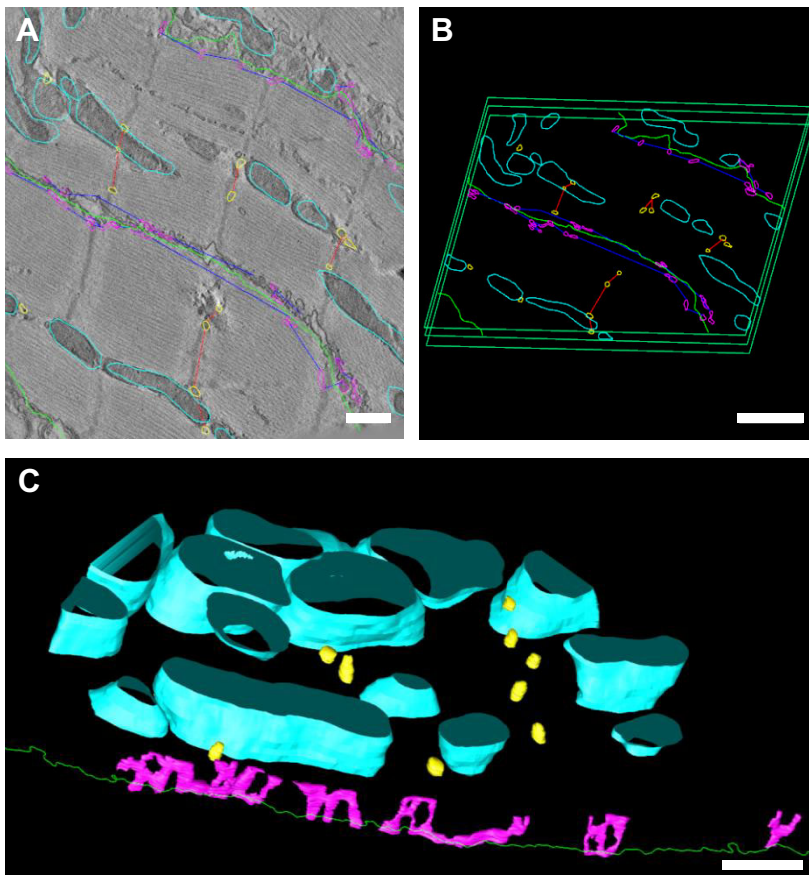$$J_n = -k_n^+[Ca^{2+}]_i([B_n]_{total} - [CaB_n]) + k_n^-[CaB_n], \quad (3)$$

Fig. 1. Tomograms and segmented structural models used for measuring inter-Ca²⁺ release unit (CRU) distance in avian left atrial tissue. (A) 2D image from a reconstructed tomogram stack, with a segmented model overlaid. The segmented model shows: peripheral couplings (PCs; purple) and the nearest edge–edge distances between PCs (blue lines); corbular sarcoplasmic reticulum (cSR; yellow) and the nearest edge–edge distances between these CRUs along a Z-line (red lines). Also segmented are the mitochondria (cyan) and the sarcolemma (green lines). Scale bar: 500 nm. Note that the segmentation overlay is from a deeper region of the tomogram than the electron microscope image, which is why the lines of the segmentation and the overlay do not always align. (B) 3D segmented model. The reconstruction is approximately 400 nm thick. Scale bar: 1000 nm. (C) 3D model showing the distribution of cSR (yellow), and the peripheral SR (purple) containing PCs near the sarcolemma (green line, only segmented in a single plane). Sub-sarcolemmal mitochondria are also shown (cyan). The free SR throughout the cell that connects PCs to the cSR has also not been segmented. Scale bar: 500 nm; scale in the z-plane is approximately 400 nm.

where B_n is the buffer concentration, and CaB_n is the Ca^{2+} bound to the buffer;

$$J_{pump} = \frac{v_{max,pump}[Ca^{2+}]_i^m}{K_{m,pump} + [Ca^{2+}]_i^m}, \quad (4)$$

$$J_{leak} = -J_{pump}(c_\infty) = -\frac{v_{max,pump}c_\infty^m}{K_{m,pump} + c_\infty^m}, \quad (5)$$

where m (=3.98) is the Hill coefficient and c_∞=0.1 µmol l^{-1};

$$J_{ryr} = O \times \sigma_{ryr} \quad (6)$$

at CRU locations, where σ_{ryr} is a 10 ms pulse of 2 pA amplitude injected into the medium by the RyR at the CRU location. The variable O took values of 1 or 0 depending on whether the CRU was open or not, respectively, and was determined stochastically. The probability of O being open was assumed to be proportional to J_{pump}. Once assigned a value of 1, O retained the value for 10 ms, the open time for the CRU (Smith et al., 1998).

Statistics
Statistics were performed using GraphPad Prism with unpaired t-tests and one-way ANOVA, with Tukey *post hoc* analysis as specified in the figure legends. The threshold for statistical significance was $P<0.05$. The results are expressed as mean± s.e.m., with the number of measurements, from the number of tissue sections and the number of animals, provided in each legend. The spread of data is shown using scatter plots of individual data points with mean values overlaid.

RESULTS
Segmented model for calculating distance
Each tomogram is a reconstruction of an approximately 400 nm thick section of avian cardiac tissue (Fig. 1; Movie 1). When the tissue is sectioned longitudinally with respect to the axis of the cells, it is apparent that cSR (yellow) are localised at the Z-lines and thus are separated at roughly the length of the sarcomere (Fig. 1A,B). The 3D structural model (Fig. 1C; Movie 2) gives a representative display of cSR spread along Z-lines, as well as the entire SR network adjacent to the sarcolemma.

PCs
PCs are defined as clusters of RyRs on the surface of the jSR which are directly adjacent (10–15 nm) to LTCCs on the sarcolemma (Fig. 2A,B). The mean (±s.e.m.) nearest edge–edge distances between PCs in each of the four chambers of the heart were as follows: LA 377±19 nm (n=380), RA 347±22 nm (n=228), LV 334±26 nm (n=193), RV 462±30 nm (n=195) (n=number of
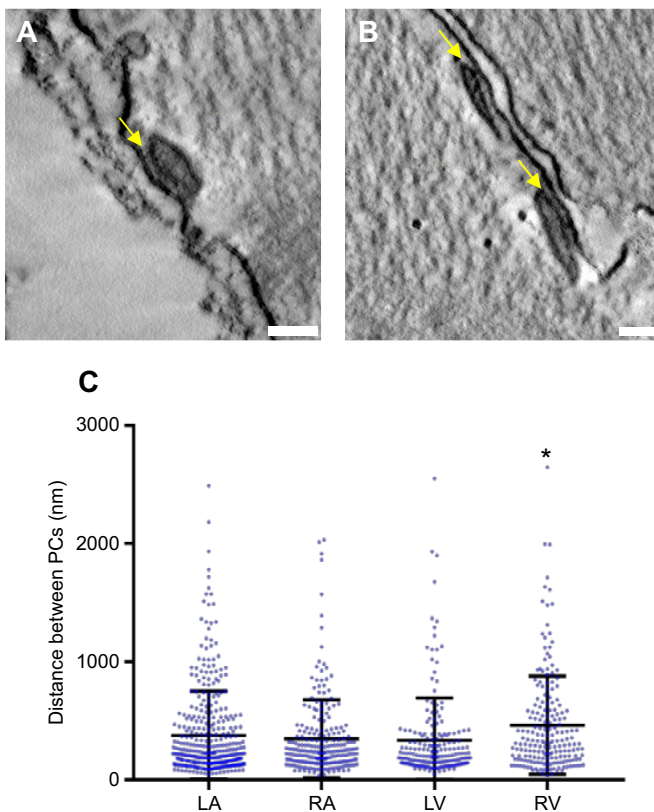

Fig. 2. PCs and inter-PC distance in avian cardiomyocytes.
(A,B) Examples of PCs (arrows) from tomograms identified as darkly stained SR cisternae that are closely opposed to the sarcolemma. Scale bars: 50 nm in both panels. (C) The nearest edge–edge distances between PCs in all four cardiac chambers. Scatter plots represent combined measurements for two birds (left ventricle, LV; right ventricle, RV) or three birds (left atrium, LA; right atrium, RA) with mean±s.e.m. overlaid. *RV was statistically different to LA, RA and LV via one-way ANOVA, with $P<0.05$. The number of distance measurements between individual PCs was as follows: n=380 LA, 228 RA, 193 LV and 195 RV.
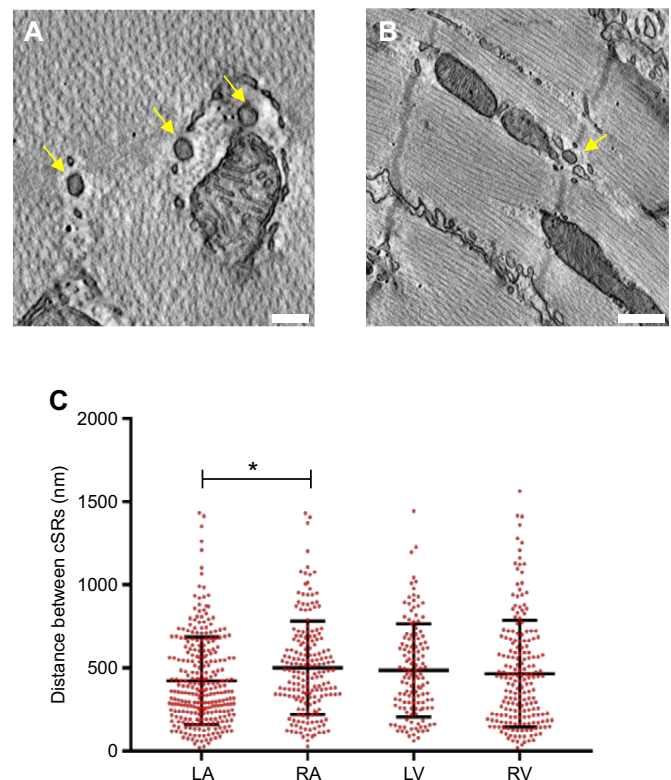

Fig. 3. cSR in avian cardiomyocytes. (A,B) Examples of cSR (arrows) from tomograms from RV (A, scale bar: 100 nm) and LA (B, scale bar: 200 nm), identified as darkly stained SR cisternae found near Z-lines, roughly 100 nm in width. (C) The nearest edge–edge distances between cSR along the same Z-line in all four cardiac chambers. Scatter plots represent combined measurements for two birds (LV, RV) or three birds (LA, RA), with mean±s.e.m. overlaid. *LA was statistically different to RA (one-way ANOVA, $P<0.05$). The number of distance measurements between cSR was as follows: n=286 LA, 189 RA, 133 LV and 194 RV.

individual distances measured; Fig. 2C). Distances between PCs in the RV were significantly greater (one-way ANOVA, $P<0.05$) than those measured in the other cardiac chambers.

cSR

The internal CRUs in avian hearts are the cSR, which are spherical structures of approximately 100 nm diameter, typically found staggered along the Z-line (Fig. 3A,B; Movie 3). cSR are notably larger in size than the network tubules of free SR (fSR); however, they are highly polymorphic in their geometry, varying in shape and size (described below). The mean (±s.e.m.) nearest edge–edge distances between cSR at the same Z-line (Fig. 3C) in each of the four chambers of the heart were as follows: LA 423±16 nm (n=286), RA 501±20 nm (n=189), LV 485±24 nm (n=133), RV 465±23 nm (n=194). Distances measured in the LA were significantly shorter than those in the RA but not different from those of the two ventricles (one-way ANOVA, $P<0.05$).

Geometric models for individual cSR

ET enables the 3D rendering of structures of interest (Fig. 4A,B). Thus, diameter (Fig. 4C), surface area (Fig. 4D) and volume (Fig. 4E) of cSR in each chamber of an individual bird heart were measured to provide insight into their role in Ca²⁺ release (Table S2). The scatterplots in Fig. 4C–E highlight the polymorphic nature of the geometry of bird cSR. The LA cSR were smaller (one-way ANOVA, $P<0.05$) in volume and surface area than those of the other chambers.

Computational modelling Ca²⁺ dynamics

To understand how inter-CRU distance may impact on Ca²⁺ activation time in an avian myocyte devoid of T-tubules, we

constructed a spatially extended 2D Ca²⁺ wave model. In the model, CRUs were placed at locations separated by distances d_1 (distance between PCs), d_2 (distance between Z-lines) and d_3 (distance between cSR along a Z-line) (Fig. 5A). Frames from a simulation of Ca²⁺ waves show the mode of diffusion across the cell, with [Ca²⁺] initially increasing at the periphery before diffusion into the interior along the Z-lines (Fig. 5B).

CRU distance in the model was varied in a systematic way to encompass the range of values measured in the tomograms, in order to deduce the effect on whole-cell activation time (Fig. 6). This analysis suggests that distance between PCs (d_1) has little effect on whole-cell Ca²⁺ activation time (Fig. 6A). In contrast, when the distance between cSR (d_3) is increased from 0.1 µm to 0.2 µm, activation time is delayed by approximately 3.5 ms; as d_3 is increased to 0.4 µm, activation time is more than 10 ms longer than that at 0.1 µm (Fig. 6B). At larger d_3 distances (beyond those measured between cSR within a Z-line in the current study), activation time is slowed even further. Under these conditions, widely separated PCs (d_1) compound the effect and activation time requires approximately 20 ms. In general, activation time is unaffected as the distance between Z-lines is varied (d_2) in a manner anticipated during sarcomeric stretch and contraction (Fig. 6). Indeed, because distance d_3 was considerably smaller than distance d_2, the CRUs along the Z-lines activated prior to Ca²⁺ passively diffusing to neighbouring Z-lines that were not proximal to the PCs.

DISCUSSION

Aves occupy a unique position in vertebrate evolution. They possess a four-chambered heart with a fully divided ventricle, which arose
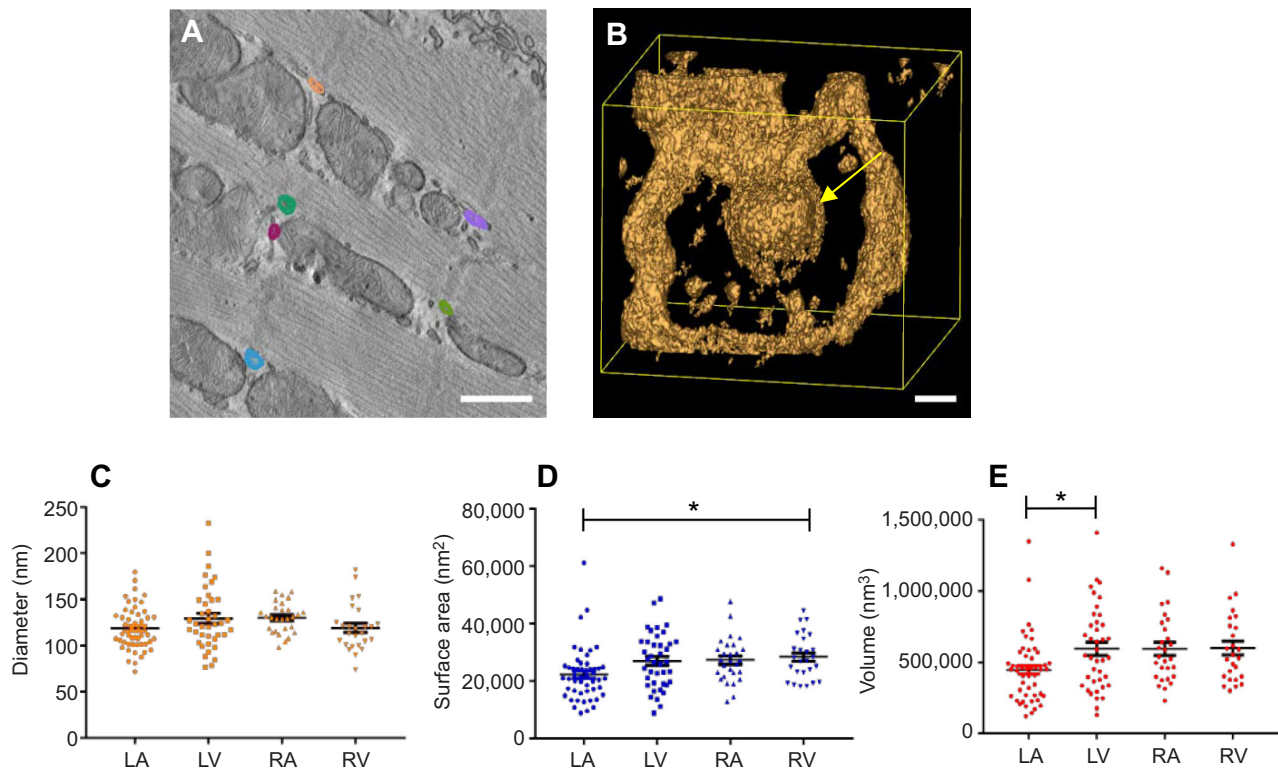

Fig. 4. Geometric models of the cSR in avian myocardium. (A) 3D segmented cSR (various colours). Scale bar: 1000 nm. (B) Isosurface rendering of an individual cSR (arrow), attached to the free SR network. Scale bar: 50 nm. (C–E) Scatterplots show the spread of the data for (C) diameter, (D) surface area and (E) volume of individual cSR, in the four chambers of the heart with mean±s.e.m. overlaid. The same data are tabulated in Table S2. Measurements were performed in all four chambers from a bird heart; n=50 LA, 40 RA, 28 LV and 26 RV. Statistical analyses showed LA was statistically different to RV in D and LA was statistically different to LV in E.
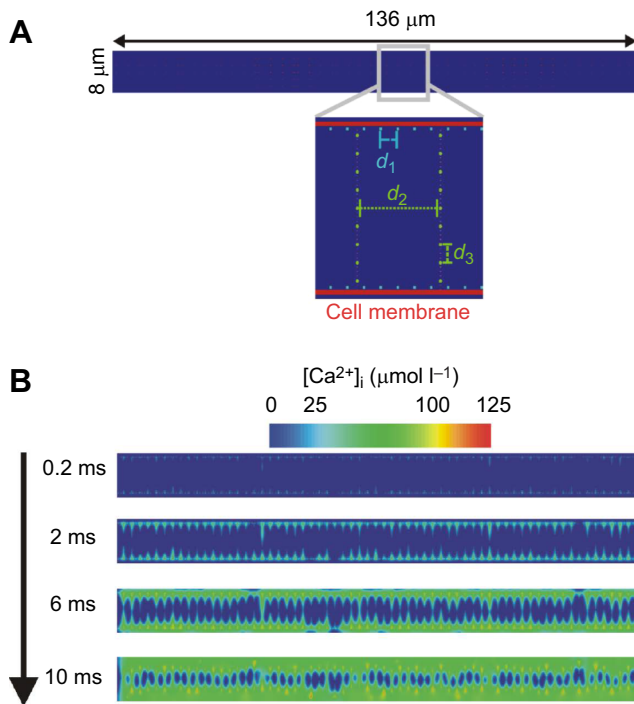
Fig. 5. Simulated cell activation time and direction of Ca^{2+} wave propagation. (A) 2D model geometry showing distance between CRUs (d_1: distance between PCs; d_2: distance between Z-lines; and d_3: distance between cSR along a Z-line, in µm). (B) Representative frames from a simulation of Ca^{2+} waves. Top panel shows stimulation at the cell membrane. In the remaining panels, Ca^{2+} diffuses from Ca^{2+} release sites to neighbouring sites and induces Ca^{2+} release at the adjacent neighbouring sites, leading to whole-cell Ca^{2+} activation.

independently from that in mammals. However, despite gross structural similarities to mammalian hearts, at a cellular level, the avian cardiomyocyte more closely resembles that of (non-avian) reptiles. This study is the first to use ET to investigate the subcellular distribution of the intracellular Ca^{2+} release machinery in the avian heart. We measured distances between PCs and between cSR along a Z-line, and found the PCs to be closer together and the cSR further apart than those reported previously using 2D TEM (Franzini-Armstrong et al., 1999; Perni et al., 2012). Our study has also revealed the diversity of cSR volumes and the varied distribution of these structures in all four cardiac chambers. We used a computational approach to test how varying the distance between these subcellular CRUs affects Ca^{2+} activation time. Our model highlights the importance of the distance between cSR along a Z-line (d_3). Together, our findings suggest that cSR clustered close together along the Z-line are vital for rapid propagation of the Ca^{2+} signal from the cell periphery to the cell centre, and facilitate strong and fast contractions.

PC distances
CRUs in the form of PCs have been identified in the hearts of all vertebrates studied, except in the frog ventricle, and are most often associated with the Z-lines (Shiels and Galli, 2014). The mean distance between nearest neighbour PCs in the white leghorn chicken ranged from 334 nm in the LV to 462 nm in the RV, which is comparable to previous values measured using 2D TEM in the LV [472 nm (Franzini-Armstrong et al., 1999) and 567 nm (Perni et al., 2012)]. We found similar distances between PCs in the LV, RA and LA but slightly longer distances in the RV. The functional

significance of this pattern is unclear. Size and frequency of peripheral CRUs vary between vertebrate species and between cardiac chambers within a species, and in some studies this variability has been related to the efficacy of excitation–contraction coupling (Perni et al., 2012; Shiels and Galli, 2014). Indeed, animals with high heart rates (i.e. finch and rat, resting heart rate ~300–350 beats min^{-1}) have closer PCs than animals with slower heart rates (Perni et al., 2012) [i.e. chicken, resting heart rate ~200 beats min^{-1}; lizard and fish, heart rate dependent on temperature but generally below 120 beats min^{-1} (Farrell, 1991)]. The distances measured in our study support previous work in chicken (Perni et al., 2012), which suggests PCs are activated by adjacent LTCCs in the sarcolemmal membrane directly, with little spread of activating Ca^{2+} longitudinally between PCs. Indeed, our simulations suggest that changing the distance between PCs between 250 and 750 nm has little impact on whole-cell activation, particularly when the distances between cSR are narrow (Fig. 6). This differs from mammalian atrial myocytes and from birds with faster heart rates and/or contractile force (i.e. finch; Perni et al., 2012), where extensive and propagative CICR between neighbouring CRUs at the cell periphery has been observed (Chen-Izu et al., 2006). In the finch heart, closely packed PCs are further aided by a higher density of LTCCs (Bogdanov et al., 1995) to achieve fast heart rates.

cSR distance
The CRUs of the avian cSR can be thought of as Ca^{2+} release relay stations, carrying the wave of Ca^{2+} from the myocyte periphery to the cell centre in the absence of T-tubules. We found the average distance between cSR at the same Z-line to range from 422 nm in the LA, to 500 nm in the RA, which are significantly larger than those reported by Franzini-Armstrong's group for the LV [148 nm (Franzini-Armstrong et al., 1999) and 235 nm (Perni et al., 2012)] using 2D TEM images taken in a transverse section. Franzini-Armstrong et al. (1999) state that 'larger distances were ignored' in their measurements, so although the exact threshold used for excluding large distances is not specified, it may explain the discrepancy between studies. The heterogeneous distribution of organelles (e.g. mitochondria), combined with changes in the distance between organelles during the contraction–relaxation cycle are both features that help prevent circular, endless propagation of a Ca^{2+} wave. Indeed, our computational model indicates that the distance between cSR has a dramatic effect on the activation time. As cSR distance is varied from those measured previously (~150–235 nm) to those measured in our study (~400–500 nm), activation time more than doubles (Fig. 6). Thus, chains of closely distributed cSR at a Z-line increase the probability that Ca^{2+} will be able to diffuse and activate neighbouring units.

cSR geometry
We provide the first 3D geometrical description of cSR in chicken hearts. A similar diverse and polymorphic description has been detailed for the jSR and the T-tubule lattice in mouse cardiomyocytes (Hayashi et al., 2009). Average diameters for cSR from each of the four chambers ranged from 120 to 130 nm, a parameter that aided cSR identification. The average volume of a cSR in each of the four chambers ranged from 446,000 to 600,000 nm^3, but the largest and smallest ranged from 120,000 to 1,410,000 nm^3. The average surface area from each of the four chambers ranged from 22,000 to 28,000 nm^2 but the extremes were 9000 nm^2 and 60,000 nm^2. Thus, there is extreme heterogeneity in the avian cardiomyocyte's Ca^{2+} release structures.
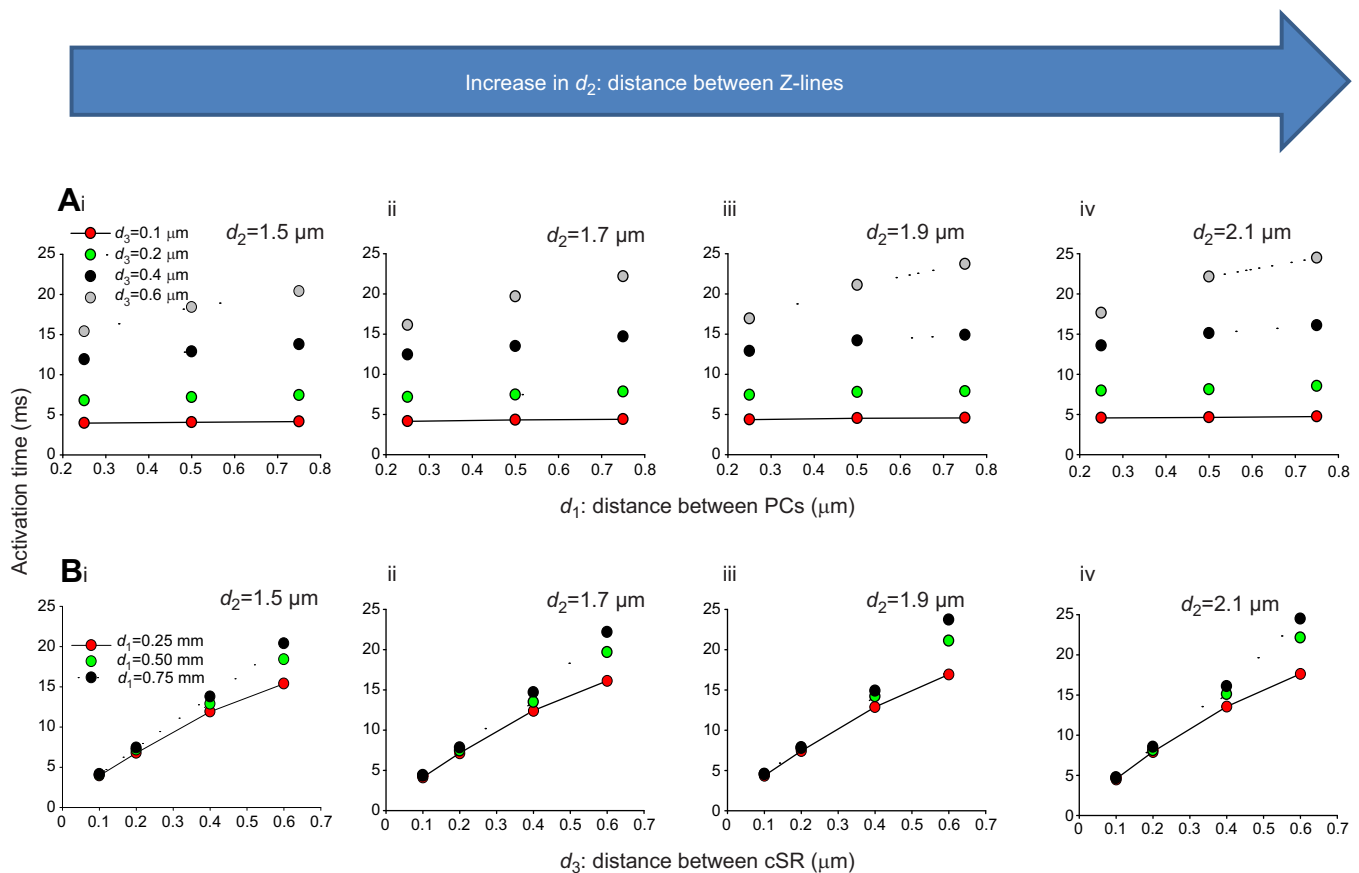
Fig. 6. Output of a 2D avian cell model showing activation time as a function of distance. (A) d_1, distance between PCs. (B) d_3, distance between cSR along a Z-line. Within each panel (i–iv), the relationship is plotted as d_2 (distance between Z-lines) is increased. The distance of d_2 was varied to represent Z-line spacing indicative of a myocyte at rest (1.7–1.9 µm), as well as encompassing values that could be achieved during myocardial stretch (2.1 µm) and during myocardial contraction (1.5 µm). In each graph, the circles represent the averaged result of 10 simulations. Each simulation required 24 processors for 4 h.

We were unable to resolve individual RyR positions on the cSR in this study. However, given the average surface area of cSR was between 22,000 and 28,000 nm², and knowing that a single RyR is 29×29 nm², or 841 nm² (Chen-Izu et al., 2006; Baddeley et al., 2009), we calculate that the average chicken cSR could support between 26 and 33 RyR molecules. RyRs probably do not occupy the entire cSR surface; for instance, the dyad is only partially filled, and RyR clusters often present a checkerboard appearance (Baddeley et al., 2009; Asghari et al., 2014). We therefore estimate the average cSR possesses approximately 13–16 RyRs.

Calculations concerning jSR Ca²⁺ capacity (whereby jSR of volume $7×10^{-4}$ µm³ contains 21,000 Ca²⁺ ions; Sobie et al., 2002), lead us to suggest the average avian cSR would contain between 13,380 and 18,000 Ca²⁺ ions. The minimum and maximum volumes of cSR found here would thus contain 3600 and 42,300 Ca²⁺ ions, respectively. A 1 pA current releases around 3000 Ca²⁺ ions per millisecond (Sobie et al., 2002), and thus the total capacity of the cSR analysed in this study permits Ca²⁺ release for ~5 ms in total before the SR is depleted of Ca²⁺. SR Ca²⁺ available for release at these CRUs is replenished by SERCA Ca²⁺ uptake along the fSR network, which diffuses back towards the junctional area containing the RyRs. Thus, the total capacity of the cSR does not finitely dictate the duration of Ca²⁺ release. It is likely that the total capacity can be released in the order of tens of milliseconds, correlating with previous measurements for known spark durations (Sobie et al., 2002; Stern et al., 2013) although the actual spark duration in avian cardiomyocytes is not known. These estimates correlate with the

Ca²⁺ activation time of our model, which ranges between 5 and 25 ms, with a mean of ~15 ms, for the whole cell to be activated, depending on CRU spacing.

Ca²⁺ dynamics model

We used a spatially extended 2D cell model to improve the interpretation of our experimental data. The model showed that the variation of distances between cSR within a Z-line supersedes that of distances between PCs at the cell membrane for setting Ca²⁺ activation time of the cell. Our model has limitations that need to be considered when interpreting our results. First, stimulation was assumed to be generated by a rapidly propagating electrical pulse along the length of the cardiomyocyte membrane. Therefore, the initiated Ca²⁺ wave had an inward propagation. Thus, barring any numerical and boundary condition effects, it may be expected that PCs played a limited role in the output of whole-cell Ca²⁺ activation. Our model also incorporated local stochastic Ca²⁺ release, or sparks. The Ca²⁺ released by the sparks diffused in the cytoplasm uniformly in all directions; thus, the Ca²⁺ diffusing from a cSR would stimulate release from the directly adjacent CRU along the same Z-line prior to stimulating other CRUs. In previous studies, inter-CRU distance was assumed to be uniform in both the x- and y-direction, thus the work here extends these earlier models (Izu et al., 2001, 2013). However, in our model the locations of the CRUs were assumed to be symmetric, which aligns with the positioning along the Z-lines that we observed experimentally in the bird heart. However, stochasticity in the spatial distribution of

CRUs has been observed (Qu et al., 2014), and will be included in future studies. Lastly, because of the limited functional studies on Ca^{2+} dynamics in avian myocytes (Kim et al., 2000), the model was parameterised based on mammalian data. Further functional studies are need to accurately measure Ca^{2+} flux in avian cardiomyocytes. Improved numerical schemes and solvers are also required to permit exploration of the experimental data in more depth. However, peak systolic Ca^{2+} was reached in a similar time frame and at a similar level in our model and that in mammals (Bers, 2002), despite the difference in cell structure between species.

Perspectives for avian cardiac performance

Domestic chickens have an average heartbeat of 218 beats min^{-1} (Prosheva et al., 2015). A single cardiac cycle is ~0.275 s and composed of the following electrocardiogram components: P wave (atrial depolarisation) ~30 ms, PQ interval ~60 ms (AV conduction), QRS (ventricular depolarisation) ~30 ms, and QT interval (duration of the ventricular action potential) ~140 ms (Prosheva et al., 2015). Ca^{2+} release follows the depolarising wave and thus our mean Ca^{2+} activation time of 12–20 ms is within a reasonable range. In the scenario where cSR distance is at or beyond the level we observed in our tomographic data, activation time would be closer to 25–30 ms. However, *in vivo*, the rate of Ca^{2+} removal and SR replenishment will also influence the speed of the calcium cycle, as an increase/decrease in heart rate is predominantly dictated by the duration of the interval between T and P waves (Dzialowski and Crossley, 2015). Functional studies are required in avian myocytes to reveal the complexities of Ca^{2+} signalling in this cell type; for instance, the speed of Ca^{2+} extrusion and specific channel currents.

In birds with faster heart rates, such as the finch or hummingbird, rapid cardiac contraction relies on even faster relaying of the Ca^{2+} signal. This is brought about by closer spacing of CRUs, and in the case of the finch heart, the existence of EjSR in place of cSR (Perni et al., 2012). EjSR are more elongated CRUs, which might offer a greater capacity for Ca^{2+} storage, increased numbers of RyRs per cluster for Ca^{2+} release, or a better geometry for the spread of signal to neighbouring sites.

Conclusions

Our measurements of distance between PCs and between cSR, coupled with computational simulations, suggest that in chicken cardiomyocytes the Ca^{2+} transient would be initiated at the periphery, be large in concentration around this sub-sarcolemmal space, and diffuse toward the interior along chains of cSR. The resulting effect would be spatial inhomogeneity and non-synchronous spread of Ca^{2+} across the whole myocyte. However, upon activation of many CRUs, given that the Ca^{2+} flux is of large enough magnitude, diffusion between cSR positioned at adjacent Z-lines is possible, becoming more probable the closer they are to one another. This pattern is similar to that found in neonatal mammalian myocytes (Louch et al., 2015). As noted by others previously (Perni et al., 2012), the extensive and almost exclusive location of cSR along the Z-lines in bird myocytes induces a high degree of refractoriness to longitudinal Ca^{2+} wave propagation, with activation initiated independently at PCs cascading through the cSR. Thus, the organisation of CRUs and the short diffusional distance for Ca^{2+} transport in narrow cells allows for strong and fast contractions in avian myocytes and reinforces the connection between structural organisation of the myocyte, the CRUs, and the strength and rate of cardiac contraction across vertebrate classes.

References

Akester, A. R. (1981). Intercalated discs, nexuses, sarcoplasmic reticulum and transitional cells in the heart of the adult domestic fowl (Gallus gallus domesticus). *J. Anat.* **133**, 161-179.

Asghari, P., Schulson, M., Scriven, D. R. L., Martens, G. and Moore, E. D. W. (2009). Axial tubules of rat ventricular myocytes form multiple junctions with the sarcoplasmic reticulum. *Biophys. J.* **96**, 4651-4660.

Asghari, P., Scriven, D. R. L., Sanatani, S., Gandhi, S. K., Campbell, A. I. M. and Moore, E. D. W. (2014). Nonuniform and variable arrangements of ryanodine receptors within mammalian ventricular couplons. *Circ. Res.* **115**, 252-262.

Baddeley, D., Jayasinghe, I. D., Lam, L., Rossberger, S., Cannell, M. B. and Soeller, C. (2009). Optical single-channel resolution imaging of the ryanodine receptor distribution in rat cardiac myocytes. *Proc. Natl. Acad. Sci. USA* **106**, 22275-22280.

Bers, D. M. (2002). Cardiac excitation-contraction coupling. *Nature* **415**, 198-205.

Bogdanov, K. Y., Ziman, B. D., Spurgeon, H. A. and Lakatta, E. G. (1995). L- and T-type calcium currents differ in finch and rat ventricular cardiomyocytes. *J. Mol. Cell. Cardiol.* **27**, 2581-2593.

Boyden, P. A., Pu, J., Pinto, J., Ter Keurs, H. E. and J, D. (2000). Ca(2+) transients and Ca(2+) waves in purkinje cells role in action potential initiation. *Circ. Res.* **86**, 448-455.

Cannell, M. B., Cheng, H. and Lederer, W. J. (1995). The control of calcium release in heart muscle. *Science* **268**, 1045-1049.

Chen-Izu, Y., Mcculle, S. L., Ward, C. W., Soeller, C., Allen, B. M., Rabang, C., Cannell, M. B., Balke, C. W. and Izu, L. T. (2006). Three-dimensional distribution of ryanodine receptor clusters in cardiac myocytes. *Biophys. J.* **91**, 1-13.

Cheng, H., Lederer, W. J. and Cannell, M. B. (1993). Calcium sparks: elementary events underlying excitation-contraction coupling in heart muscle. *Science* **262**, 740-744.

Deerinck, T. J., Bushong, E., Thor, A. and Ellisman, M. H. (2010). NCMIR methods for 3D EM: a new protocol for preparation of biological specimens for serial block face scanning electron microscopy. *Nat. Center Microsc. Imag. Res.* **6**.

Dibb, K. M., Clarke, J. D., Horn, M. A., Richards, M. A., Graham, H. K., Eisner, D. A. and Trafford, A. W. (2009). Characterization of an extensive transverse tubular network in sheep atrial myocytes and its depletion in heart failure. *Circ. Heart Fail.* **2**, 482-489.

Dzialowski, E. M. and Crossley, D. A., II (2015). Chapter 11-The cardiovascular system. In *Sturkie's Avian Physiology*, 6th edn (ed. C. G. Scanes), pp. 199-201. San Diego: Academic Press.

Farrell, A. P. (1991). From hagfish to tuna: a perspective on cardiac function in fish. *Physiol. Zool.* **64**, 1137-1164.

Franzini-Armstrong, C., Protasi, F. and Ramesh, V. (1999). Shape, size, and distribution of Ca(2+) release units and couplons in skeletal and cardiac muscles. *Biophys. J.* **77**, 1528-1539.

Franzini-Armstrong, C., Protasi, F. and Tijskens, P. (2005). The assembly of calcium release units in cardiac muscle. *Ann. N. Y. Acad. Sci.* **1047**, 76-85.

Hayashi, T., Martone, M. E., Yu, Z., Thor, A., Doi, M., Holst, M. J., Ellisman, M. H. and Hoshijima, M. (2009). Three-dimensional electron microscopy reveals new details of membrane systems for Ca2+ signaling in the heart. *J. Cell Sci.* **122**, 1005-1013.

Izu, L. T., Wier, W. G. and Balke, C. W. (2001). Evolution of cardiac calcium waves from stochastic calcium sparks. *Biophys. J.* **80**, 103-120.

Izu, L. T., Xie, Y., Sato, D., Bányász, T. and Chen-Izu, Y. (2013). Ca(2+) waves in the heart. *J. Mol. Cell. Cardiol.* **58**, 118-124.

Junker, J., Sommer, J. R., Sar, M. and Meissner, G. (1994). Extended junctional sarcoplasmic reticulum of avian cardiac muscle contains functional ryanodine receptors. *J. Biol. Chem.* **269**, 1627-1634.

Kharche, S. R., Vigmond, E., Efimov, I. R. and Dobrzynski, H. (2017). Computational assessment of the functional role of sinoatrial node exit pathways in the human heart. *PLoS ONE* **12**, e0183727.

Kim, C. S., Doye, A. A., Gwathmey, J. K., Davidoff, A. J. and Maki, T. M. (2000). Intracellular calcium and the relationship to contractility in an avian model of heart failure. *J. Comp. Physiol. B Biochem. Syst. Environ. Physiol.* **170**, 295-306.

Kremer, J. R., Mastronarde, D. N. and Mcintosh, J. R. (1996). Computer visualization of three-dimensional image data using IMOD. *J. Struct. Biol.* **116**, 71-76.

Louch, W. E., Koivumaki, J. T. and Tavi, P. (2015). Calcium signalling in developing cardiomyocytes: implications for model systems and disease. *J. Physiol.* **593**, 1047-1063.

Mirsalimi, S. M., O'brien, P. J. and Julian, R. J. (1993). Blood volume increase in salt-induced pulmonary hypertension, heart failure and ascites in broiler and White Leghorn chickens. *Can. J. Vet. Res.* **57**, 110-113.

Perni, S., Iyer, V. R. and Franzini-Armstrong, C. (2012). Ultrastructure of cardiac muscle in reptiles and birds: optimizing and/or reducing the probability of transmission between calcium release units. *J. Muscle Res. Cell Motil.* **33**, 145-152.

Prosheva, V., Dernovoj, B., Kharin, S., Kaseva, N., Shklyar, T. and Blyakhman, F. (2015). Does the right muscular atrioventricular valve in the avian heart perform two functions? *Comp. Biochem. Physiol. A Mol. Integr. Physiol.* **184**, 41-45.

Qu, Z., Hu, G., Garfinkel, A. and Weiss, J. N. (2014). Nonlinear and stochastic dynamics in the heart. *Phys. Rep.* **543**, 61-162.

Shiels, H. A. and Galli, G. L. (2014). The sarcoplasmic reticulum and the evolution of the vertebrate heart. *Physiology* **29**, 456-469.

Shiels, H. A. and White, E. (2005). Temporal and spatial properties of cellular Ca2+ flux in trout ventricular myocytes. *Am. J. Physiol. Regul. Integr. Comp. Physiol.* **288**, R1756-R1766.

Smith, G. D., Keizer, J. E., Stern, M. D., Lederer, W. J. and Cheng, H. (1998). A simple numerical model of calcium spark formation and detection in cardiac myocytes. *Biophys. J.* **75**, 15-32.

Sobie, E. A., Dilly, K. W., Dos Santos Cruz, J., Lederer, W. J. and Jafri, M. S. (2002). Termination of cardiac Ca(2+) sparks: an investigative mathematical model of calcium-induced calcium release. *Biophys. J.* **83**, 59-78.

Sobie, E. A., Guatimosim, S., Gómez-Viquez, L., Song, L.-S., Hartmann, H., Jafri, M. S. and Lederer, W. J. (2006). The Ca(2+) leak paradox and "rogue ryanodine receptors": SR Ca(2+) efflux theory and practice. *Prog. Biophys. Mol. Biol.* **90**, 172-185.

Sommer, J. and Johnson, E. (1969). Cardiac muscle. *Zeitschrift für Zellforschung und Mikroskopische Anatomie* **98**, 437-468.

Sommer, J. R. (1995). Comparative anatomy: in praise of a powerful approach to elucidate mechanisms translating cardiac excitation into purposeful contraction. *J. Mol. Cell. Cardiol.* **27**, 19-35.

Stern, M. D., Ríos, E. and Maltsev, V. A. (2013). Life and death of a cardiac calcium spark. *J. Gen. Physiol.* **142**, 257-274.

Stuyvers, B. D., Dun, W., Matkovich, S., Sorrentino, V., Boyden, P. A. and ter Keurs, H. E. D. J. (2005). Ca2+ sparks and waves in canine purkinje cells: a triple layered system of Ca2+ activation. *Circ. Res.* **97**, 35-43.

Woo, S.-H., Cleemann, L. and Morad, M. (2003). Spatiotemporal characteristics of junctional and nonjunctional focal Ca^{2+} release in rat atrial myocytes. *Circ. Res.* **92**, e1-e11.